KSME

Springer

Journal of Mechanical Science and Technology 36 (7) 2022

Original Article
DOI 10.1007/s12206-022-0637-1

Keywords:
· Coating quality
· CGDS
· Explicit time integration
· Particle impingement
· Thermal effect

Correspondence to:
Lin Zhu
zl009@mail.ustc.edu.cn

# These authors equally contributed to this work as first author.

Citation:
Dong, S.-J., Ye, J., Zhu, L., Guo, L., Moray, P. J., Liu, W.-L., Sun, J., Jen, T.-C. (2022). Thermal effect of high-velocity particle impingements on coating quality in cold gas dynamic spray operations. Journal of Mechanical Science and Technology 36 (7) (2022) 3619~3629. http://doi.org/10.1007/s12206-022-0637-1

Received November 25th, 2021
Revised February 24th, 2022
Accepted March 3rd, 2022

† Recommended by Editor Hyung Wook Park

Thermal effect of high-velocity particle impingements on coating quality in cold gas dynamic spray operations

Si-Jia Dong[1,#], Jian Ye[2,#], Lin Zhu[1,3], Li Guo[4], Peter Jusu Moray[1], Wei-Lai Liu[5], Jun Sun[6] and Tien-Chien Jen[7]

[1]Lab of Mechanical Structure and Biomechanics, School of Engineering, Anhui Agricultural University, Hefei 230036, China, [2]Department of Physics, School of Science, Anhui Agricultural University, Hefei 230036, China, [3]Anhui Province Engineering Laboratory of Intelligent Agricultural Machinery and Equipment, Hefei 230036, China, [4]School of Food Science and Engineering, Qilu University of Technology, Jinan 250300, China, [5]Department of Precision Machinery and Precision Instrumentation, University of Science and Technology of China, Hefei 230027, China, [6]Department of Orthopedics, Anhui Provincial Children's Hospital, Hefei 230051, China, [7]Mechanical Engineering Department, University of Johannesburg, Johannesburg 2006, South Africa

Abstract This investigation is aimed to evaluate thermal effects of the high-velocity particle impingement on the coating quality in CGDS (cold gas dynamic spray). To achieve this, the authors used an explicit time integration approach to predict interface temperatures and deformation profiles of the substrate, as well as, their relationship in commercial solver ABAQUS 6.13. Copper (Cu) and aluminum (Al) materials were specified to particle and substrate, respectively. Two essential process parameters, including six different impact velocities (300, 400, 500, 600, 700, 800 m/s) and three different particle sizes (1, 5, 15 μm), were involved in all simulations. There are very good agreements between the simulated and the published that the non-uniform interface temperature and the poor/failure particle deposition have the direct relationship with either impact velocity or particle size. Once again this study strongly demonstrates the thermal effect of the high-velocity particle impingement on coating quality in CGDS, in turn providing insights into process parameter selection.

1. Introduction

Cold gas dynamic spray (CGDS) is an emerging additive manufacturing (AM) technique, in which micro/nano material particles are speeded up, by the supersonic gas flow, at significantly low temperatures, and subsequently deposited onto a substrate with high-velocity impact (Fig. 1), as reported by Viscusi et al. [1]. Rahmati et al. [2] concluded that the high-velocity impact generally results in uniform coat over the substrate surface through large plastic deformation at significantly high strain rates.

Actually there exist thermal spray operations, e.g., arc spray in the manufacturing industry besides the CGDS, as indicated by Assadi et al. [3]. Raoelison et al. [4] claimed that the biggest advantage of CGDS, different from the thermal spray technique, is that the coated particles during the spray are not molten, retain their original properties and thus improve product qualities. For this reason, the CGDS is being widely used for various engineering applications, particularly in defense and aerospace sectors.

For the better CGDS application, currently numerous attempts have been carried out with different methods including experimental, analytical and numerical analyses to understand the underlying physical mechanism in CGDS and improve the coating quality. These attempts are primarily focused on two distinct categories—material suitability and process parameter. For the material suitability, Moridi et al. [5] found that low yield strength materials, e.g., copper and aluminum are appropriate for the CGDS applications due to their high softening properties at the

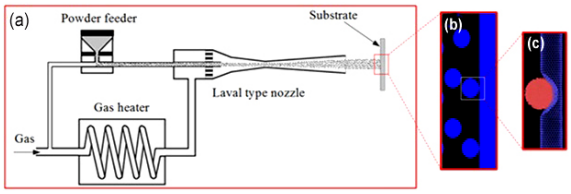

Fig. 1. CGDS process: (a) experimental setup; (b) magnified image of the particle impact onto the substrate; (c) further magnified image of (b) showing substrate material deformation.

elevated impact temperature, however, high strength materials are not ideal for not enough energies in CGDS coat them the substrate. For the process parameters, e.g., impact velocity and particle size, Yen et al. [6] claimed that the accelerating capability of carrier gases is dependent of the categories and the distance between nozzle and substrate. These investigations are beneficial for an ample variety of the CGDS applications, but more detailed analyses are needed to implement the thermal effects of the particle impingement on coating quality. This can be explained as follows: the high-velocity particle impact onto the substrate surely results in the high interface temperature due to so much energy conversion, and simultaneously the plastic deformation caused by the particle impact is highly concentrated in a very small zone at a very short period; from the viewpoint of heat transfer and material mechanics, this combined effect of the high interface temperature, very small deformation zone and very short period may produce non-uniform temperature and strain at the interfacial zone, which is likely to produce poor/failure deposition, e.g., the scraping on the substrate; consequently, this scraping can strongly affect the coating quality in CGDS.

Actually, investigating the thermal effect of the particle impact on the coating quality in CGDS has been occasionally reported. Schmidt and Wong et al. selected copper for the particle, aluminum for the substrate, and then investigated the relationship between interface temperature and bonding possibility. They demonstrated the feasibility of the particle bonding onto the substrate as the impingement temperature reaches 60 % of the material melting point [7, 8]. King et al. reported the effects of stagnation temperature and substrate hardness on particle deformation and adhesion. They confirmed that for the same particle material, i.e., copper and different substrate materials, i.e., commercial purity (CP) aluminum and alloy 7050-T7451, the particle deposition efficiency is increased with the stagnation temperature [9]. However, notwithstanding these meaningful findings, to the best of our knowledge, the degree to which the high-velocity particle impingement thermally affects the coating quality is still a recent research focus.

For this reason, the current study is concerned with the thermal effects of the high-velocity particle impingement on the coating quality in CGDS for two essential process parameters, i.e., the six different impact velocities and three different particle sizes. In particular, the aims are to (1) numerically investigate the thermal influence mechanism and the thermal effect of the essential process parameters, and (2) validate the thermal model in this study and further assess the thermal effect by comparing the obtained numerical results with the published data in literature. In terms of copper and aluminum materials specified as the particle and substrate in this study, the criterion on the minimum bonding temperature, from Schmidt and Wong et al., was chosen for all simulations. In their studies the minimum bonding temperature for copper material is 650 °C.

Table 1. Material properties of particle and substrate [8, 10].

Material		Cu	Al
Density	kg/m^3	8960	2700
Thermal conductivity	W/(m·K)	386	20
Specific heat	J/(kg·°C)	383	920
Melting point	°C	1083	643
Elastic modulus	GPa	124	65.8
Poisson's ratio		0.34	0.30
JC plasticity		90, 292, 0.31	148.36, 345.51
		0.025, 1.09	0.18, 0.001, 0.86
JC damage		0.54, 4.89	0.071, 1.248
		-3.03, 0.014, 1.12	-1.142, 0.147, 1
Reference temperature	°C	25	25
Reference strain rate	s^{-1}	1	1

2. Materials and methods

2.1 Material properties

In an attempt to compare the calculations in this study and the published date in literature, the materials of particle and substrate for all simulations were taken from Wong and Yen et al. [8, 10]. That is, copper was selected as the particle material, and aluminum as the substrate material. Their relevant properties are listed in Table 1.

2.2 Computational approach

For the cases examined in this paper, the centered difference time integrate approach was used in an explicit finite element method based commercial solver ABAQUS 6.13 as a modelling platform. The thermal effects of the particle impingement on the coating quality at the varying impact velocities and particle sizes were assessed through the deformation profiles and temperature variations on the particle-substrate interface as well as their relationship. All numerical results presented here refer to the data obtained after 60 ns of calculations, which were ever used by Wong, Yen and Sunday Temitope Oyinbo and Jen et al. [8, 10, 11].

2.2.1 Mathematical models

More generally, mechanics of the high deformation impingement is strongly affected by the plastic flow of the material. In order to accurately evaluate the aforementioned relationship the combined bilinear Johnson-Cook (JC) flow stress with dynamic failure model was applied to the high-velocity particle

impingement in CGDS in this study. This is dominantly due to the former better representing the interface temperature rise compared to the other models for high-strain-rate material deformation and the latter effective dealing with progressive damage and materials failure, which are reported by Chen et al. and Yildirim et al. [12, 13]. More detailed comparison on the high-strain-rate material deformation models is available in the Ref. [12].

The bilinear JC flow stress can be calculated by:

$$\sigma_Y = (A + B\varepsilon_p^n)\left(1 + C\ln\frac{\dot{\varepsilon}_p}{\dot{\varepsilon}_0}\right)\left(1 - \left(\frac{T - T_R}{T_m - T_R}\right)^m\right), \text{ with}$$

$$C = \begin{cases} C_1 \quad and \quad \dot{\varepsilon}_0 = 1 \quad if\, \dot{\varepsilon}_p < \dot{\varepsilon}_c \\ C_2 \quad and \quad \dot{\varepsilon}_0 = \dot{\varepsilon}_c \quad if\, \dot{\varepsilon}_p > \dot{\varepsilon}_c \end{cases} \tag{1}$$

where A, B, C, n, and m are the material parameters, ε_p —the equivalent plastic strain, $\dot{\varepsilon}_p$ —the equivalent plastic strain rate, $\dot{\varepsilon}_0$ —the reference strain rate, T_m —the melting temperature of the material, T_R —the reference temperature.

The JC dynamic failure model is arisen from the equivalent plastic strain at element integration points. Assume that the failure appears when the damage parameter ω is greater than 1. Thus, the ω can be calculated by:

$$\omega = \sum\left(\frac{\Delta\bar{\varepsilon}^{pl}}{\bar{\varepsilon}^{pl}}\right), \text{ with}$$

$$\bar{\varepsilon}^{pl} = \left[d_1 + d_2\exp\left(d_3\frac{p}{q}\right)\right]\left[1 + d_4\ln\left(\frac{\dot{\bar{\varepsilon}}^{pl}}{\dot{\varepsilon}_0}\right)\right](1 + d_5\hat{\theta}) \tag{2}$$

where $\Delta\bar{\varepsilon}^{pl}$ is an increment of equivalent plastic strain, $\bar{\varepsilon}^{pl}$ —the strain at failure, $\dot{\bar{\varepsilon}}^{pl}/\dot{\varepsilon}_0$ —a non-dimensional strain rate, p/q— a dimensionless pressure-deviatoric stress ratio (p is the compressive stress; q is the Mises stress), d_1~d_5—failure parameters, $\dot{\varepsilon}_0$ —the reference strain rate, $\hat{\theta}$ —the non-dimensional temperature.

Coulomb friction model was used to evaluate the relationship between the maximum allowable stress and the contact pressure at the interface. The simple Coulomb friction law is presented below:

$$\tau^* = \tau_f\left(1 - \left(1 - \frac{\delta - \delta_0}{\delta_c - \delta_0}\right)^n\right) \tag{3}$$

where τ^* is frictional traction, τ_f —the maximum fractional traction, δ —the shear separation, δ_0 —the shear separation corresponding to the maximum shear separation, δ_c —the critical shear separation. Detailed information on the Coulomb friction model is available in the Ref. [14].

To calculate the conversion between plastic deformation energy and heat energy, we used the following Ref. [15]:

$$\int_{T_0}^{T}\rho c_p dT = \beta\int_{\varepsilon_{p0}}^{\varepsilon_p}\sigma d\varepsilon \tag{4}$$

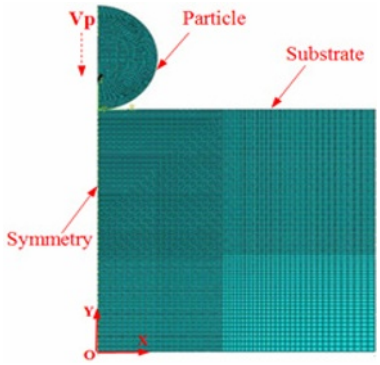

Fig. 2. Computational model for particle impact onto the substrate.

where the subscript '0' means an initial value, β —the inelastic heat fraction, T— the particle impact temperature, ε —the deformation strain, p —the stress due to pressure. Note that the value in β was set to 0.9 in this study. This is because for copper and aluminum materials 90 % of the deformation energy is approximately transformed into heat energy, claimed by Grujicic et al. [16].

In addition, for good accuracy the comparisons between various energy components were also involved in the analysis of the particle impingement. These energy components include internal energy, internal heat, viscous, and frictional energies etc., reported by Gao et al. [17].

2.2.2 Numerical simulations

For all simulations, we based on Li and Gao [15] and implemented the following simplicity and assumptions: 1) the impact velocity perpendicular to the substrate surface; 2) negligible gravity influence; 3) ninety percent of plastic work converted into heat; and 4) one hundred percent of friction work converted into heat.

In this study a two-dimensional (2D) model was used to investigate the thermal effect mechanism on the particle impingement onto the substrate and evaluate the thermal influence of the essential process parameters on the coating quality in CGDS. In this model, the particle and the substrate were modelled to be a solid circle and a rectangle, respectively; the particle sizes were specified as 5, 10, and 15 μm, respectively; the length and height of the substrate were set three and four times greater than the particle radius, respectively. These settings have been demonstrated that the waves reflecting from the boundaries do not interfere with the contact and rebound behaviours at all, reported by Wong et al. [8]. It should be noted that the half of the 2D model was used for all simulations due to the axisymmetric structure and due to the reduced computational cost. For the half model, the outer and bottom boundaries of the substrate were fixed, and symmetric conditions were imposed on the axis Y as shown in Fig. 2.

In order to further obtain accurate results and save calculation time, different mesh strategies were applied for the various sections of the particle and substrate, respectively. To achieve this, we partitioned the substrate into two zones. The

first is referred to the impingement zone where dense meshes were used. The second is the non-impingement zone where sparse meshes were used because of no significantly large material deformation happening. The two mesh zones were connected by the mesh tie constraints, which enable all the freedom degrees from the both sides to conform to each other during the simulations, conclude by Hussain et al. [18]. The detailed mesh strategy is presented below: the same mesh size was specified for the impingement zone between particle and substrate, the nominal mesh size was 1/55 of the particle diameter, and the impingement zone was approximately as large as one-half of the rectangular length; away from the impact zone was used a coarser mesh, whose size was five times as large as the mesh size in the impact zone. The quad structure mesh used in the FEA model was created by using the four-node bilinear elements. Note that the mesh strategy used here has been demonstrated to be feasible and effective by a series of mesh convergence tests, reported by Wong and Yen [8, 10].

For all the cases examined in this study, the boundary condition on conduction heat transfer was included in the particle impingement process for evaluating its thermal effect, in which the coupled temperature-displacement explicit approach, proposed by Schmidt et al. [7], was used. This explicit time integration scheme has been demonstrated to better deal with such the significantly complex and nonlinear interactions as large deformation and plasticity in CGDS, as reported by Chen et al. [12]. Considering the contact properties between particle and substrate, we used the general contact algorithm to simulate the particle-substrate interaction; a line-to-line 'Hard' contact model was applied for the contact pair, which is predominantly due to the fact that it can minimize the penetration of the particle surface into the substrate surface, claimed by Chen et al. [12]. To reduce or avoid the excessive unrealistic element distortion caused by the high-velocity impingement, enhanced hourglass control was used by Wong [8].

The initial velocity and size of the particle were dependent on the cases studied in this paper. The specified particle impact velocities were 300, 400, 500, 600, 700, 800 m/s, and particle sizes were 1, 5, 15 μm. The friction coefficient on the particle-substrate interface was assumed to be identical and assigned as 0.2. The initial temperature used for particle and substrate was 25 °C. Note that the thermal effect arising from the high-velocity particle impingement on the mass densities of the particle and the substrate material were not taken into account for all simulations.

3. Results and discussions

In terms of the objective of this study—the thermal influence mechanism and the thermal effect of high-velocity impingements on the coating quality in CGDS, the numerical simulations are concerned with the following two aspects. The first is referred to the thermal influence mechanism, in which the relationship between impact temperature and deformation

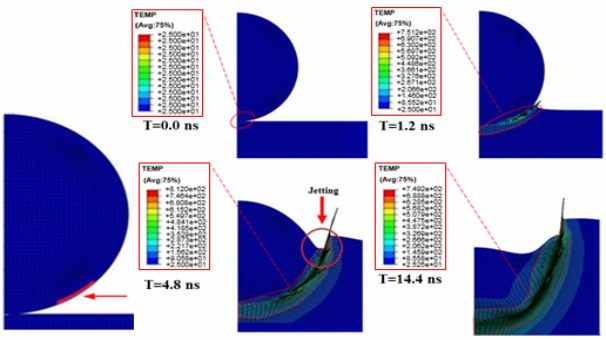

Fig. 3. The 5 μm particle impact onto the interface at 700 m/s.

evolution on the interface was investigated at the impingement velocity of 700 m/s and particle size of 5 μm. The reason why these parameters were chosen is to compare these calculations with the published CGDS measurements, which were obtained at the same settings. The second is referred to assess the thermal effects of the particle impingement, in which the interface temperature profiles, deformation evolutions as well as their relationship were investigated at the different impact velocities and different particle sizes, respectively.

3.1 Thermal effect mechanism

Fig. 3 shows instant deformation profiles and temperature variations (°C) at the monitored strain zone along the particle-substrate interface at 700 m/s impact velocity with 5 μm particle size. As observed, the whole deformation evolution experiences three phases: 1) localized shear strain at T = 1.2 ns, caused by the impact stress gradient; 2) distinctive deformations with material jetting at the interface edge at T=4.8 ns; 3) particle bonding on the substrate at T = 14.4 ns. with the deformation evolutions the interface temperatures are varied as follows: initially, 25.0 °C at T = 0.0; subsequently, 751.2 °C at T = 1.2 ns; then, 812 °C at T = 4.8 ns; finally, 749.2 °C at T = 14.4 ns.

The most critical deformation in Fig. 3 is material jetting, as indicated by the red arrow, which may be caused by the combined effects of great strain rate and high interface temperature in CGDS. In detail, the abrupt stop of particle impingements produces distinctive deformation pattern and localized shear stress at the interface edge, where a rather small volume at the impingement zone becomes unstable due to plasticity-induced heating; more generally, the particle deformation is sufficiently dependent of the flow stress variation because of the strain, strain-rate hardening and thermal softening caused by the severe material plasticity; the thermal softening effect is greater than the strain and strain-rate hardening effects, which causes the yield stress of particle material to significantly drop [19-21]; Consequently, the relatively high interface temperature, e.g., 800 °C in this case causes the material atoms of this impingement zone to flow like a fluid, thereby contributing to the rapid expanding and jetting of the particle material from the center zone to the interface

Table 2. Maximum interface temperature (T_{max}) at the varying impingement velocities (V) and particle sizes (D).

T_{max} (°C)	D = 1 μm	D = 5 μm	D = 15 μm
V = 300 m/s	247.6	328.4	355.5
V = 400 m/s	353.0	468.7	544.8
V = 500 m/s	394.6	511.5	601.7
V = 600 m/s	487.5	696.1	866.4
V = 700 m/s	529.0	790.6	928.2
V = 800 m/s	689.6	879.8	1100.0

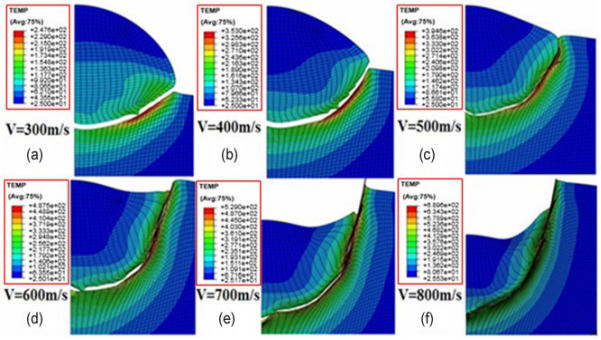

Fig. 4. Interface temperature and deformation profiles of 1 μm particle at the varying impingement velocities.

edge. From this analysis, it follows that the rapid increase in local interface temperature rise, due to the particle impingement, greatly influences the particle-substrate interface deformation. This deformation is demonstrated to be associated with the coating qualities in CGDS.

3.2 Thermal effect

3.2.1 Thermal effect of impingement velocity

Figs. 4-6 schematically show the final deformation profiles and temperature distributions along the particle-substrate interface at the impact velocities (V) of 300, 400, 500, 600, 700 and 800 m/s, corresponding to the particle sizes (D) of 1, 5 and 15 μm. The relevant maximum values in interface temperature are listed in Table 2.

As Figs. 4(a)-(e) reveal, the 1 μm particles whose impact velocities are smaller than 800 m/s are all unable to efficiently bond onto the substrate. These phenomena could be demonstrated by the chinks appearing in the middle of the particle-substrate interface. As the impact velocity is increased to 800 m/s, however, no chink exists any more, meaning that the particle has successfully bonded onto the substrate (Fig. 4(f)). Further comparison of the Figs. 4(a)-(e) indicates that the corresponding maximum interface is 529.0 °C, not exceeding 60 % of the melting temperature of copper, i.e., 650 °C, and that the maximum interface temperature in Fig. 4(f) is 689.6 °C. Similar phenomena are also found in Figs. 5 and 6, in which the maximum interface temperatures of the 5 and 15 μm particles, successfully bonding onto the substrate, are all larger than 650 °C. To take an example, for the 5 μm particle the

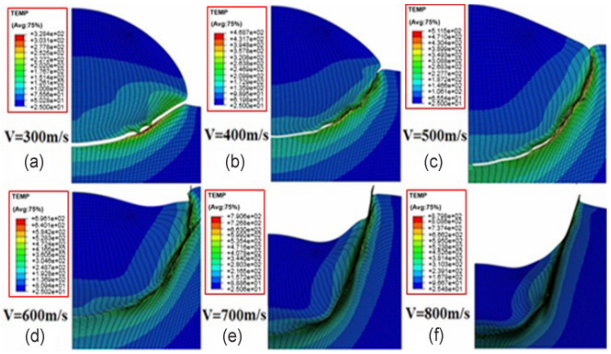

Fig. 5. Interface temperature and deformation profiles of 5 μm particle at the varying impingement velocities.

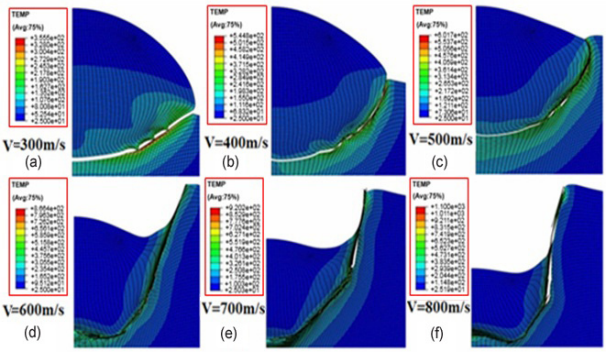

Fig. 6. Interface temperature and deformation profiles of 15 μm particle at the varying impingement velocities.

corresponding maximum interface temperatures are 696.1 °C at 600 m/s, 790.6 °C at 700 m/s, and 879 °C at 800 m/s, respectively; for the 15 μm particle the maximum interface temperatures are 866.4 °C at 600 m/s, 920.2 °C at 700 m/s, and 1100 °C at 800 m/s. It follows that the relationship between interface temperature and coating effectiveness in this study is in good agreement with the work of Schmidt and Wong depicted in the Introduction Section. However, it should be noted that for the 15 μm particle there exists the chink at the interface margin either at 700 m/s or 800 m/s (Figs. 6(e) and (f)). This is likely due to the great flow stress variation developed at the coating-substrate interface at significantly high temperatures because of very different elastic moduli and thermal expansion coefficients.

In order to better evaluate the thermal effects of the impact velocity, it is particularly necessary to investigate the temperature variation at the monitored strain zone along the particle-substrate interface in the entire bonding process [22-24]. The monitored strain zone is shown in Fig. 3. Figs. 7-9 schematically show the relationship between impact velocity and interface temperature at the monitored strain zone in the entire impingement process for the different particle sizes, respectively. Table 3 indicates the times when the interface temperarures reach the bonding temperature for the six different velocitiies ranged between 300 and 800 m/s with three different partizle sizes. As observed, for the constant particle

Table 3. Critical time reaching bonding temperature for different impact velocities.

Time (ns)	300 m/s	400 m/s	500 m/s	600 m/s	700 m/s	800 m/s
1 μm	×	×	×	×	×	1.4
5 μm	×	×	×	7.8	3.6	2.6
15.0 μm	×	×	×	22.2	15	9.8

Note: The sign '×' indicates that the maximum impact temperature do not reach 650 °C.

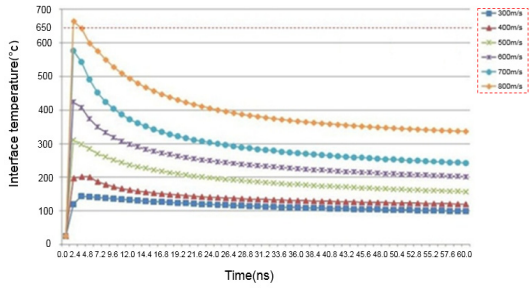

Fig. 7. Interface temperature evolutions of 1 μm particle at the varying impingement velocities.

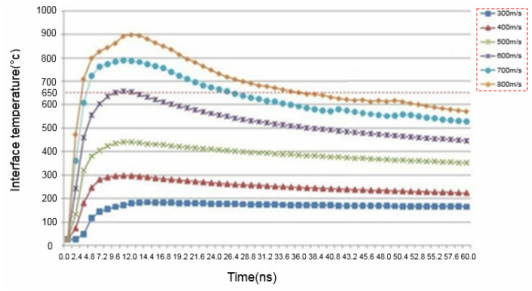

Fig. 8. Interface temperature evolutions of 5 μm particle at the varying impingement velocities.

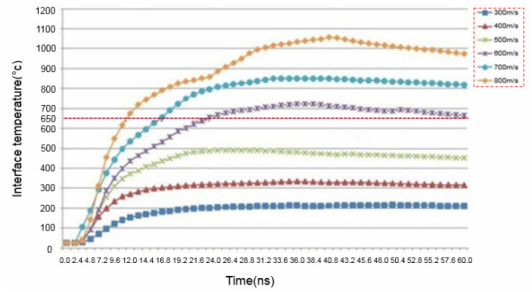

Fig. 9. Interface temperature evolutions of 15 μm particle at the varying impingement velocities.

size all the interface temperatures show the similar variation trend. That is, these temperatures increase the maximum values firstly and then decease as the impact velocity increases. However, there exists the discrepancy that the interface temperature increases and decreases more rapidly with the smaller particle size. These phenomena could be demonstrated by the plot slops, illustrated in Figs. 7-9. These results may be attributed to the less thermal energy converted from the smaller particle at the same impingement velocity. Figs. 7-9 also agree with the numerical results in Figs. 4-6 that any particle whose interface temperature exceeds 650 °C is able to successfully bond onto the substrate.

Based on Figs. 4-9, it is inferred that the impact velocity has strong thermal effects on the coating through the interface temperature. This is mainly due to the fact that the great kinetic energy can significantly decrease the deposition height and flattening ratio due to particle penetrating into the substrate, thereby producing the shear plastic deformation and affecting the bonding possibility of the adjacent materials.

3.2.2 Thermal effect of particle size

Figs. 10-15 show the interface temperature variations in the entire bonding process at the particle sizes of 1, 5 and 15 μm with six impact velocities of 300, 400, 500, 600, 700 and 800 m/s, respectively. Note that this interface temperature variation occurs at the monitored strain zone along the particle-substrate (Fig. 3). Table 4 indicates the times when the interface temperarures reach the bonding temperature for the three particle sizes ranged 1 and 15 μm with the six different velocitiies.

As observed, for the constant impact velocity all the plots of the interface temperature indicate the similar variation—increasing firstly and then deceasing with the simulation time; and furthermore the interface temperature increases and decreases more rapidly as the particle is getting smaller. To take an example, for the particle sizes of 1, 5 and 15 μm in Fig. 15, the first times to reach the minimum bonding temperature, i.e., 650 °C are approximately 1.4, 2.6 and 9.8 ns, respectively; upon the maximum temperature the plot of 1μm particle deceases most rapidly, which could be demonstrated by the plot slops in Fig. 15. In addition, Figs. 10-15 also agree with the numerical results in Figs. 4-6 that any particle whose interface temperature exceeds 650 °C is able to successfully bond onto the substrate.

As can be inferred from Figs. 10-15, the particle size significantly affects the interface temperature. This may be attributed to the combined influence of the initial kinetic energy due to impingement and the particle size associated with energy dissipation. In detail, for the same impact velocity the bigger particle size on the one hand results in the more kinetic energy, while on the other, the impact of the bigger particle onto the substrate produces both the higher plastic strain rate and the greater adiabatic shear instability [25, 26]. The higher plastic strain may cause the interface temperature to slowly rise; the greater adiabatic shear instability is accompanied with the larger interfacial jets, which can hold the particle strongly and hence prevent the interface temperature from decreasing rapidly [27].

From the FE predictions in Figs. 4-15, it is inferred that the high-velocity impingement may have adverse thermal effects on the coating quality in CGDS through the development of non-uniform temperature and deformation at the interfacial zone.

Table 4. Critical time reaching bonding temperature for different partical sizes.

Time (ns)	1 μm	5 μm	15.0 μm
300 m/s	×	×	×
400 m/s	×	×	×
500 m/s	×	×	×
600 m/s	×	7.8	22.2
700 m/s	×	3.6	15
800 m/s	1.4	2.6	9.8

Note: The sign '×' indicates that the maximum imapct temperatures do not reach 650 °C.

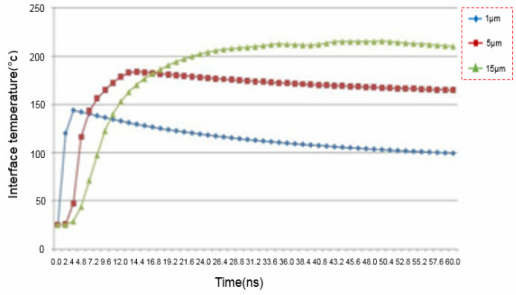

Fig. 10. Interface temperature variations at the different particle sizes and 300 m/s impingement velocity.

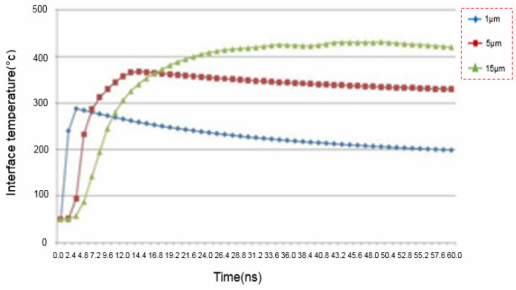

Fig. 11. Interface temperature variations at the different particle sizes and 400 m/s impingement velocity.

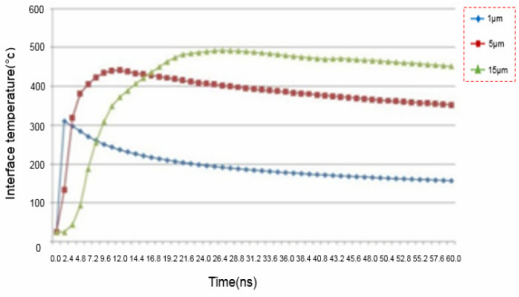

Fig. 12. Interface temperature variations at the different particle sizes and 500 m/s impingement velocity.

4. Comparison of results with published findings

Based on the numerical results attained in Sec. 3, this section is concerned with the following two comparisons: first, validating the thermal model in this study; and second, further assessing the thermal effect. For the first validation, since the test set-up in CGDS for a single particle impact is not constructed in the lab, the thermal model is validated by comparing the numerical results in this study and the published

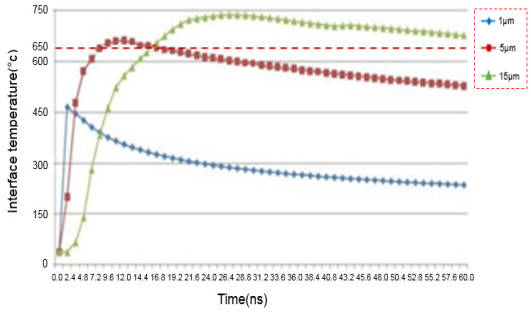

Fig. 13. Interface temperature variations at the different particle sizes and 600 m/s impingement velocity.

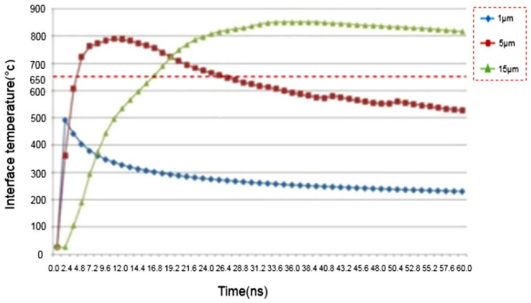

Fig. 14. Interface temperature variations at the different particle sizes and 700 m/s impingement velocity.

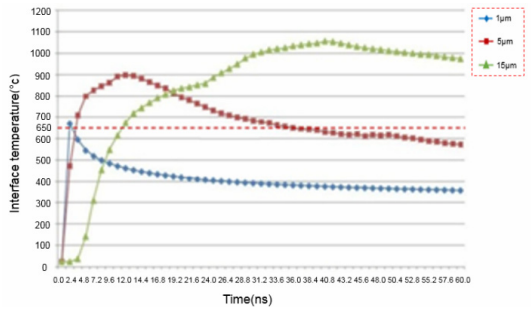

Fig. 15. Interface temperature variations at the different particle sizes and 800 m/s impingement velocity.

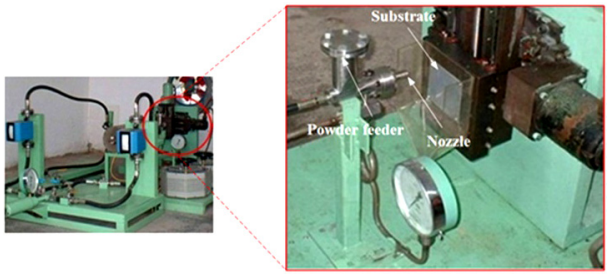

Fig. 16. Experimental setup of CGDS [10].

Table 5. Maximum interface temperature (Tmax) from Wong [8].

T_{max} (°C)	D = 1μm	D = 5 μm	D = 15 μm
V = 600 m/s	×	657.0	×
V = 800 m/s	687.0	×	×

Note: The sign '×' indicates that the maximum impact temperatures do not reach 650 °C.

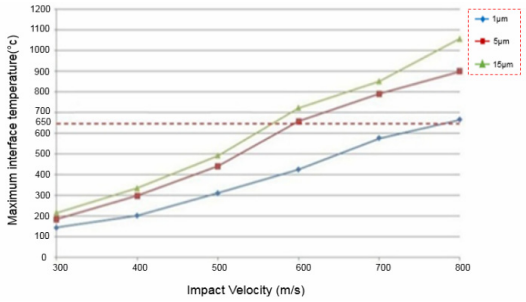

Fig. 17. Maximum interface temperature at the different particle sizes and impingement velocities.

numerical findings. The published simulations were implemented by Wong [8]. For the second evaluations, the numerical results in this study were compared with the published experimental findings at the same settings in literature. The published measurements were performed by Yen [10], in which the test set-up in CGDS is schematically illustrated in Fig. 16.

4.1 Comparison of the results with published numerical findings

Fig. 17 shows the maximum interface temperatures at the six different impact velocities of 300, 400, 500, 600, 700, and 800 m/s with three different particle sizes of 1, 5, 15 μm. The Table 5 presents the maximum interface temperatures at the two different impact velocities of 600, 800 m/s with three different particle sizes of 1, 5, 15 μm, reported by Wong [8]. The characters V and D in Table 5 indicate the particle impingement velocity and particle diameter, respectively. Note that the published interface temperatures presented here were attained at the identified particle and substrate material properties with those in this study. We refer the readers to the work of Wong for details of the simulations.

As observed, the predicted maximum interface temperatures have the same variation trends as the published numerical findings: 1) for the identical impingement velocity, i.e., 600 m/s, the maximum interface temperature is increased with the particle size; 2) for the 1 μm particle, the maximum interface temperatures at 800 m/s exceed the minimum bonding temperature 650 °C, the results from Schmidt et al.; and 3) there are few discrepancies in interface temperature value (see Fig. 17 and Table 5). For example, the predicted maximum interface temperatures in this study are approximately 670 °C at 800 m/s, 660 °C and 720 °C at 600 m/s, respectively,

Table 6. Particle sizes and impact velocities used in the Ref. [10].

Particle size (μm)	1	5	15	25	30
Impact velocity (m/s)	618.9	751.4	522.0	418.33	306.0

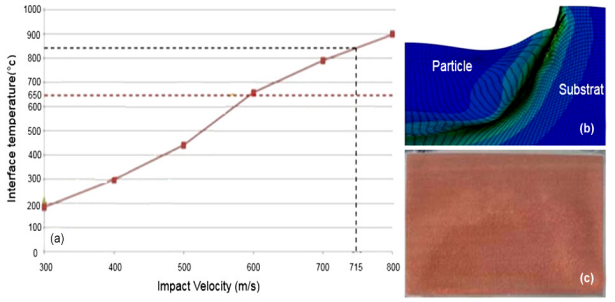

Fig. 18. Comparison between numerical and experimental result for 5 μm particle: (a) the interface temperature at varying impact velocity; (b) particle-substrate bonding profile; (c) the bonding result of 5 μm particles.

corresponding 1, 5, 15 μm. Compared to the numerical results in Table 5, the relevant discrepancies are -2.54 %, 0.45 %, and -0.28 %, respectively. Hence, it is concluded that there are very good agreements between the predicted and the published numerical results for the thermal model in this study.

4.2 Comparison of the results with published experimental findings

The published experimental findings were attained in the test set-up shown in Fig. 16, where the elliptical zone indicates the detail of de Laval nozzle, substrate and power feeder of the set-up. Copper (Cu) and aluminum (Al) materials, same as those in this study, were specified to the particle and the substrate in all tests, respectively; the impact velocities and the particle sizes involved in this experiment are listed in Table 6; itrogen was used as the carrier gas to transport and deposit the particles with high-velocity onto the substrate in order to protect them from oxidation; and during the entire experiment, 80 % of the particles were distributed around the selected size. More detailed information on the CGDS experiment is available in Ref. [10]. Note that only the 1 μm and 5 μm particles in Table 6 were chosen for the comparison, which is based on the numerical simulations in this study. All the simulations were implemented at the conditions identical with those in the experimental setup shown in Fig. 16.

For the 5 μm particle, Fig. 18 shows the relationship between interface temperature in this study and coating quality reported by Yen [10]. Based on our predictions, the interface temperature at the impact velocity of 715 m/s exceeds the minimum bonding temperature, i.e., 650 °C (the black dashed line in (a)), and the 5 μm particle in this case can be coated the substrate well (see (b)). As expected, the 5 μm particle did bond onto the substrate effectively, which is confirmed by good coating qualities on the substrate in the published experimental findings (see (c)).

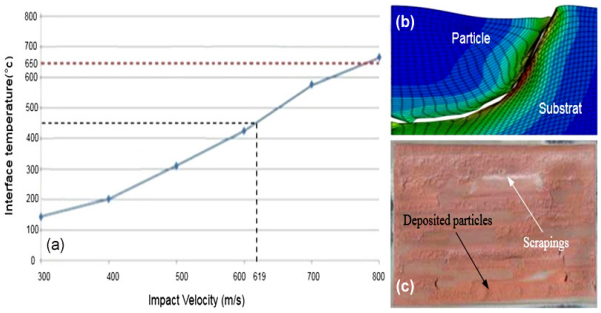

Fig. 19. Comparison between numerical and experimental result for 1 μm particle: (a) the interface temperature at varying impact velocity; (b) particle-substrate bonding profile; (c) the bonding result of 1 μm particles.

For the 1 μm particle, Fig. 19 shows the relationship between interface temperature in this study and coating quality in Ref. [10]. Based on our predictions, the interface temperature at the impact velocity of 619 m/s is smaller than the minimum bonding temperature (the black dashed line in (a)), the 1 μm particle in this case cannot be coated the substrate, and the poor or failure deposition should appear there (see (b)). As expected, some significant scraping of the coatings, indicated by the white arrow in (c), did appear in the published experimental findings (see (c)). However, it should be noted that good coating qualities were also found on some locations of the substrate (see the black arrow in (c)). This may be due to the multi-particle impingement process of CGDS, in which the particle-particle and particle-substrate interactions have strong influences on the bonding quality.

From the aforementioned comparisons, the thermal model used in this study is confirmed to be accurate enough to access the thermal effect of the high-velocity impingement in CGDS, and also it is inferred that the high-velocity particle impingement has the thermal effects on the coating quality because of the poor/failure deposition.

5. Conclusions

In this study, an explicit model based finite element method incorporating the bilinear JC flow stress, dynamic failure, and Coulomb friction models is used to investigate the underlying thermal influence mechanism on the copper particle impingement onto the aluminium substrate in CGDS. The study also assesses the thermal effects of the two essential process parameters, i.e., impact velocity and particle size on the coating quality. The major findings of this study can be summarized as follows.

1) The impact velocity study shows that the maximum interface temperature is increased with the increase in impact velocity—for example, for the 5 μm particle the maximum interface temperature is increased from 328 °C to 880 °C with the increase of impact velocity from 300 m/s to 800 m/s. The impact velocity is believed to have strong thermal effects on the coating through the interface temperature. This is mainly due to the fact that the great kinetic energy can significantly decrease the deposition height and flattening ratio due to particle penetrating into the substrate, thereby producing the shear plastic deformation and affecting the bonding possibility of the adjacent materials.

2) The particle size study shows the significant effects on the interface temperature—for example, the peak interface temperatures of 1, 5 and 15 μm particles are approximately 675 °C, 900 °C, and 1050 °C, respectively. This is because of the combined influence of the initial kinetic energy due to high-speed impingement and the particle size associated with energy dissipation.

The study on thermal influence mechanism reveals that the rapid increase in local interface temperature due to the high-velocity particle impingement has strong influences on the particle deformation evolution in CGDS through the initial kinetic energy conversion and dissipation. During this process the highly coupled strain, strain-rate hardening and thermal softening appear on the particle-substrate interface and most importantly the thermal softening effect is much stronger than the strain and strain-rate hardening. Consequently, this coupled phenomenon develops the material instability and produces the shear plastic deformation, thereby affecting the bonding quality. The FE based results in this study are consistent with the published numerical results and experimental evidences in literature. Our comparisons have demonstrated the effectiveness of the thermal model for the prediction of the coating quality and also confirmed the thermal effects of the high-velocity particle impingement on the coating quality in CGDS. Due to the multi-particle impingement phenomenon of the CGDS and based on the current calculations, the future numerical predictions will be extended to the three-dimensional multi-particle impact for more thorough thermal effects on the coating quality in CGDS.

Acknowledgments

We would like to thank the reviewers for their hard work. And also we acknowledge financial support for this work from the National Natural Science Foundation of China (52175211, 52005009), the Key Research and Development Project of Anhui Province (202004a06020015, 202004e11020003), the Major Programs of Anhui Provincial Education Department (KJ2020ZD09), Anhui Provincial Natural Science Foundation (2108085ME164), as well as the Opening Fund of the Anhui Province Engineering Laboratory of Intelligent Agricultural Machinery and Equipment.

References

[1] A. Viscusi, P. Ammendola, A. Astarita, F. Raganati, F. Scherillo, A. Squillace, R. Chirone and L. Carrino, Aluminum foam made via a new method based on cold gas dynamic sprayed powders mixed through sound assisted fluidization technique, *Journal of Materials Processing Technology*, 231 (2016) 265-

276.
[2] S. Rahmati, A. Zúñiga, B. Jodoin and R. G. A. Veiga, Deformation of copper particles upon impact: a molecular dynamics study of cold spray, *Computational Materials Science*, 171 (2020) 109-219.
[3] H. Assadi, H. Kreye, F. Gärtner and T. Klassen, Cold spraying-a materials perspective, *Acta Materialia*, 116 (2016) 382-407.
[4] R. N. Raoelison, E. Aubignat, M. P. Planche, S. Costil, C. Langlade and H. Liao, Low pressure cold spraying under 6 bar pressure deposition: exploration of high deposition efficiency solutions using a mathematical modelling, *Surface Coating Technology*, 302 (2016) 47-55.
[5] A. Moridi, S. M. Hassani-Gangaraj, M. Guagliano and M. Dao, Cold spray coating: review of material systems and future perspectives, *Surface Engineering*, 36 (2014) 369-395.
[6] Y. H. Yen, S. C. Wong, T. C. Jen, Q. H. Chen and Q. Liao, The effects of optimized nozzle-substrate distance on cold gas dynamic spray (CGDS) process, *Proceeding of ASME International Mechanical Engineering Congress and Exposition*, 7 (2012) 353-361.
[7] T. Schmidt, H. Assadi, F. Ga¨rtner, H. Richter, T. Stoltenhoff, H. Kreye and T. Klassen, From particle acceleration to impact and bonding in cold spraying, *Journal of Thermal Spray Technology*, 18 (2009) 794-808.
[8] S. C. Wong, Thermal analysis of the particle critical velocity on bonding efficiency in cold gas dynamic spray, *Master Thesis,* University of Wisconsin-Milwaukee (2010).
[9] P. C. King, G. Bae, S. H. Zahiri, M. Jahedi and C. Lee, An experimental and finite element study of cold spray copper impact onto two aluminum substrates, *Journal of Thermal Spray Technology*, 19 (2010) 620-634.
[10] Y. H. Yen, The effects of optimized nozzle-substrate distance on cold gas dynamic spray (CGDS) process, *Master Thesis*, University of Wisconsin-Milwaukee (2010).
[11] S. T. Oyinbo and T. C. Jen, Investigation of the process parameters and restitution coefficient of ductile materials during cold gas dynamic spray (CGDS) using finite element analysis, *Additive Manufacturing*, 31 (2020) 100986.
[12] Q. Chen, A. Alizadeh, W. Xie, X. Wang, V. Champagne, A. Gouldstone, J.-H. Lee and S. Müftü, High-strain-rate material behavior and adiabatic material instability in impact of micron-scale Al-6061 particles, *Journal of Thermal Spray Technology*, 27 (2018) 641-653.
[13] B. Yildirim, S. Muftu and A. Gouldstone, Modeling of high velocity impact of spherical particles, *Wear*, 270 (2011) 703-713.
[14] G. Nian, Q. Li, Q. Xu and S. Qu, A cohesive zone model incorporating a Coulomb friction law for fiber-reinforced composites, *Composites Science and Technology*, 157 (2018) 195-201.
[15] W. Y. Li and W. Gao, Some aspects on 3D numerical modeling of high velocity impact of particles in cold spraying by explicit finite element analysis, *Applied Surface Science*, 255 (2009) 7878-7892.
[16] M. Grujicic, C. L. Zhao, W. S. DeRosset and D. Helfritch, Adiabatic shear instability based mechanism for particles/substrate bonding in the cold-gas dynamic-spray process, *Material Design*, 25 (2004) 681-688.
[17] W. Gao, J. Li, Y. Li and L. Kong, Numerical identification of critical erosion prone areas in tube heat exchangers, *Engineering Applications of Computational Fluid Mechanics*, 14 (2020) 1429-1444.
[18] T. Hussain, D. G. McCartney and P. H. Shipway, Bonding between aluminum and copper in cold spraying: story of asymmetry, *Journal of Materials Processing Technology*, 28 (2012) 1371-1378.
[19] A. Joshi and S. James, Molecular dynamics simulation study of cold spray process, *Journal of Manufacturing Processes*, 33 (2018) 136-143.
[20] R. Ghelichi, S. Bagherifard, M. Guagliano and M. Verani, Numerical simulation of cold spray coating, *Surface Coating Technology*, 205 (2011) 5294-5301.
[21] M. Grujicic, J. R. Saylor, D. E. Beasley, W. S. DeRosset and D. Helfritch, Computational analysis of the interfacial bonding between feed-powder particles and the substrate in the cold gas dynamic-spray process, *Applied Surface Science*, 219 (2003) 211-227.
[22] T. C. Jen, L. Li, W. Cui, Q. Chen and X. Zhang, Numerical investigations on cold gas dynamic spray process with nano- and microsize particles, *International Journal of Heat Mass Transfer*, 48 (2005) 4384-4396.
[23] L. Zhu, T. C. Jen, Y. T. Pan and H. S. Chen, Particle bonding mechanism in cold gas dynamic spray: a three-dimensional approach, *Journal of Thermal Spray Technology*, 26 (2017) 1859-1873.
[24] S. Rahmati and A. Ghaei, The use of particle/substrate material models in simulation of cold-gas dynamic-spray process, *Journal of Thermal Spray Technology*, 23 (2014) 530-540.
[25] R. N. Raoelison, Y. Xie, T. Sapanathan, M. P. Planche, R. Kromer, S. Costil and C. Langlade, Cold gas dynamic spray technology: a comprehensive review of Processing conditions for various technological developments till to date, *Additive Manufacturing*, 19 (2018) 134-159.
[26] A. Sova, S. Grigoriev, A. Okunkova and I. Smurov, Potential of cold gas dynamic spray as additive manufacturing technology, *The International Journal of Advanced Manufacturing Technology*, 69 (2013) 2269-2278.
[27] U. Prisco, Size-dependent distributions of particle velocity and temperature atimpact in the cold-gas dynamic-spray process, *Journal of Materials Processing Technology*, 216 (2015) 302-314.

Si-Jia Dong is a master degree can didate in Department of Mechanical Engineering of Anhui Agricultural University (P.R. China). She received her B.S. from College of Economics and Technology, Anhui Aqricultural University in 2020. Her research interest is numerical simulations in fluid mechanics.

Jian-Ye is a lecturer in School of Science of Anhui Agricultural University (P.R. China). He is a Ph.D. student of theoretical physics at University of Science and Technology of China. His research interest is experimental optics.

Lin Zhu is a Professor in Department of Mechanical Engineering of Anhui Agricultural University (P.R. China). He received his Ph.D. from University of Science and Technology of China in 2008, and was ever a postdoc research associate at University of Wisconsin-Milwaukee (USA) from 2009. 2. to 2018. 8. His current research interests include structure and performance optimization of mechanical components, and microfluids.

Li Guo is a Professor in School of Food Science of Qilu University of Technology. She received her Ph.D. from Anhui Agricultural University (P.R. China) in 2009, and was ever a postdoc research associate at Purdue University. Her current research interest is mechanics in food.

Peter Jusu Moray is a master degree candidate in Department of Mechanical Engineering of Anhui Agricultural University (P.R. China). His research interest is numerical simulations in fluid mechanics.

Wei-Lai Liu is a lecturer in Precision Mechinary and Precision Instrumentation, University of Science and Technology of China. His research interest is experimental optics.

Tien-Chien Jen is a Professor in Mechanical Engineering of the University of Johannesburg, South Africa. He is Member of Academy of Science and South Africa (ASSAF) and also fellow of the American Society of Mechanical Engineering (ASME). His research interest is CGDS.

Sun Jun is a Professor in Orthopedics of Anhui Provincial Children'S Hospital. He graduated from Anhui Medical University. His research interest is mechanics in skeletal system.